Highly Efficient, Wavelength-Tunable, Gold Nanoparticle Based Optothermal Nanoconvertors

Cheng-Hsuan Chou, Cheng-Dah Chen, and C. R. Chris Wang*

Department of Chemistry and Biochemistry, National Chung Cheng University, Min-Hsiung, Chia-Yi 621, Taiwan, Republic of China

Received: December 7, 2004; In Final Form: March 17, 2005

A photon-to-thermal energy conversion nanosystem based the near-infrared irradiation of one-dimensional gold nanoparticles (nanorods) is highly efficient and tunable to the incident wavelength. Using ambient photothermal detection, we observed a temperature rise of ca. 30 °C upon irradiating an aliquot of an aqueous nanoparticle suspension with a laser for 5 s. The temperature can be elevated even higher by embedding the particles into a poorly thermally conducting solid medium. The illuminated area of a sample containing nanorod particles embedded in a polyurethane matrix can be heated to >100 °C upon irradiation for 1 min. This optothermal conversion efficiency can be turned on selectively by tuning the wavelength to match that of the surface plasmon resonance of the particles. This specificity, with respect to the wavelength of the incident light, makes these highly efficient, particle-based, optothermal nanoconvertors suitable for potential use in multicolor detection on biochips and related sensors and as ideal contrasting agents for optoacoustic biomedical imaging applications.

1. Introduction

Studies of the interactions of light with matter are of extreme scientific and technological importance. Although they have no capability to emit light as efficiently as semiconductor nanocrystals,[1−4] noble metal nanoparticles have intriguing optical properties of high absorption cross sections. For example, the absorption cross section of a 5-nm-diameter gold particle is ca. 3 nm^2 at a wavelength of 514 nm.[5] This value is more than 2 orders of magnitude higher than that of organic fluorophores at room temperature. Such high absorption cross sections in the visible range have recently stimulated many advanced studies on these materials' applications for detection of biological systems, such as the colorimetric,[6−10] scanometric,[11−14] and electrical detection of oligonucleotides.[15] The noble metal nanoparticles also exhibit many enhanced linear and nonlinear processes involving the interactions of these nanoparticles with electromagnetic radiation,[16] such as surface-enhanced Raman scattering,[17−20] and second harmonic generation.[21] Studies have also been conducted on the post-absorption ultrafast energy relaxation dynamics on these nanoparticles, such as electron−electron and electron−phonon processes and heat release.[22−24] In general, the electron energy relaxation to the phonon bath occurs on a time scale on the order of a few picoseconds. The diffusion of heat out of thin gold or silver films, for example, requires several hundred picoseconds. It is then realized that the strong optical absorption behavior of noble metal nanoparticles is capable of creating a photothermal effect, i.e., an increase in temperature around the particle when it is illuminated by laser light. Recently, photothermal imaging on gold nanospheres[25] has been demonstrated to occur as a result of their low scattering and excellent photoabsorption ability. The temperature variations were detected optically by using a sensitive interference method developed specifically for this imaging purpose. In addition to photothermal imaging, the transient thermal effect induced by interactions with electromagnetic radiation has been applied successfully to the local dehybridization of adjacent DNA strands by the use of a magnetic field oscillating at a radio frequency.[26] In this case, the working temperature that can be generated by the gold nanoparticles is typically 35 °C.

Rodlike gold nanoparticles possess several interesting light-absorbing properties, such as their extremely large photoabsorption cross sections and remarkably sensitive spectral shifts of their surface plasmon (SP) resonances as a function of the particles' elongation. We carefully calibrated the extremely large absorption coefficient of gold nanorods at the λ_{max} of their SP resonance band. For example, the absorption coefficient at 950 nm for the gold nanorods having a mean aspect ratio of 5 was measured to give ca. 5.5×10^9 $M^{-1}\cdot cm^{-1}$.[27] We anticipated that the optothermal conversion of these nanorods would be highly efficient and tunable; in this paper we describe our findings in regard to this matter.

2. Experimental Section

Experiments were performed by carefully synthesizing gold nanorods that have distinct aspect ratio distributions and conducting their thermal imaging with the use of an IR camera. The gold nanorods were synthesized by the electrochemical conversion of an anodic gold material into particles within an electrolytic cosurfactant system, a procedure that we have developed previously.[28,29] The cationic surfactants used were hexadecyltrimethylammonium bromide (CTABr) and tetradodecylammonium bromide (TDABr). The particle shape was controlled successfully by the cationic cosurfactant micelles, which included several other ingredients. The gold nanorods were then well dispersed in aqueous solutions. To allow comparisons to be made, we also synthesized suspended Au nanospheres using a similar aqueous solution, but excluding the TDABr. The structural evidence of thus-synthesized nanoparticles were obtained via transmission electron microscopy

* To whom correspondence should be addressed. E-mail: checrw@ccu.edu.tw.

10.1021/jp0444520 CCC: $30.25
Published on Web 05/12/2005

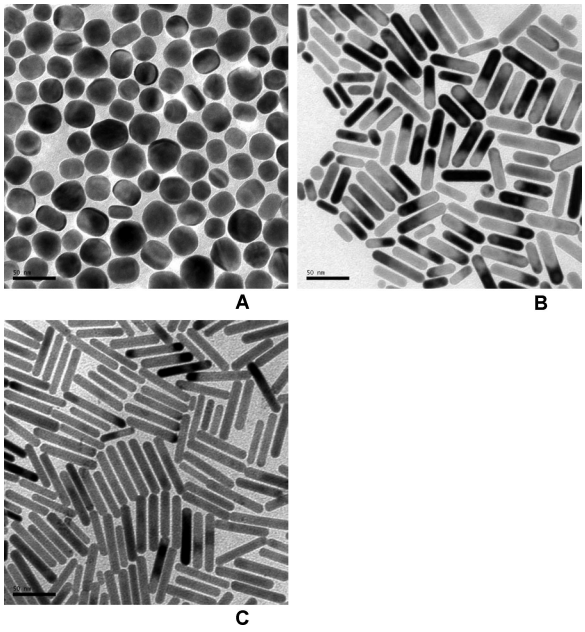

Figure 1. TEM images of gold nanoparticles having different mean aspect ratios. (A) 1.2 ± 0.2; (B) 3.9 ± 1.0; (C) 5.5 ± 0.9. Scale bar = 50 nm.

(TEM) using an accelerating voltage of 150 kV. Prior to TEM sample preparation, the colloids were pretreated through a flocculation/redispersion cycle to remove any excess coexisting compounds; we then prepared TEM samples by dip-coating Formvar/carbon film Cu grid with the colloidal solutions. The absorption spectra of these colloidal solutions or embedded film were collected on an HP 8453 ultraviolet−visible photodiode array spectrophotometer.

To illustrate the photothermal effect of the particles in parallel with their wavelength dependence, samples containing gold nanoparticles were placed between a continuous solid-state laser with output at 785 nm (laser power of 146 mW) and an IR camera (AVIO Neo Thermo TVS-610; temperature range −20 to 300 °C and resolution <0.1 °C). The laser light irradiated the samples from below from a distance of ca. 2 mm. The IR camera then recorded images from above each sample after its irradiation for a specific time. The highest temperatures in the images were recorded directly by the camera. The accuracy of this reading from the imaging camera has been carefully calibrated and its error bar is typically less than 0.2 °C.

3. Results and Discussion

Figure 1 shows distinct particle geometries of the three types of gold nanoparticles used in our studies.

Figure 2A presents an image of these samples, which are (from left to right) deionized water, gold nanospheres, and short and long gold nanorods. The concentrations of the three nanoparticle samples, which have distinct particle geometries, were adjusted to give the same absorbance of ca. 2.5 at their absorption maxima. The two nanorod samples exhibit their surface plasmon resonances at 775 and 980 nm, as indicated in Figure 2B, which correspond to mean aspect ratios of these particles of 3.9 and 5.5, respectively. The optothermal effect was imaged by illuminating each sample individually with light from a 785-nm solid-state laser for 5 s. All of the measurements were performed in such a way that the light source was placed underneath the sample and the thermal image was detected from above. Figure 2C−F presents the resulting temperature elevations, equilibrated with the room temperature of ca. 25 °C,

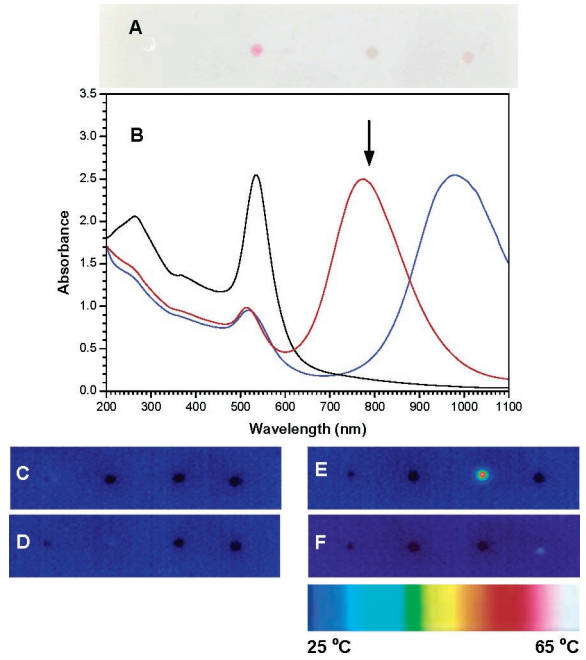

Figure 2. Optothermal conversions of three samples of gold nanoparticles and a blank. (A) Photographic image of a slide upon which four sample droplets were placed. From left to right: deionized water, gold nanospheres, and short and long gold nanorods. (B) Absorption spectra of the gold nanoparticles having mean aspect ratios of 1.2, 3.9, and 5.5, measured under an optical path length of 1.0 cm. A continuous solid-state laser with output at 785 nm (indicated by the downward arrow; laser power = 146 mW) was used to illuminate the samples (2 μL of aqueous solution) individually. The laser light irradiated the samples from below from a distance of ca. 2 mm; an IR camera (AVIO Neo Thermo TVS-610) recorded images from above each sample after its irradiation for 5 s. The thermal images corresponding to the four samples are shown in the series (C)−(F); the final temperatures at the centers of the hot spots are (C) 28.5, (D) 28.6, (E) 54.7, and (F) 31.8 °C.

arising from the photothermal effects of each of the four different samples. We observe in Figure 2C,D that no measurable temperature buildup occurred in the droplets of the first two samples, simply because they are transparent to the incident light, and thus, their low absorption cross sections resulted in an insignificant degree of thermal conversion that equilibrated rapidly under the ambient conditions.

The cw laser output heats the two gold nanorod samples and creates the radiant circular images. The most dramatic temperature increase at the center of the hot zone—ca. 26.2 °C within 5 s—is exhibited by the shorter rod sample [AuNR(775); mean aspect ratio = 3.9]. The mean aspect ratio of these nanorods was chosen so that the value of λ_{max} occurred at 775 nm, which is very close to the incident wavelength. We realized that it is a possibility that the particle shape transformation process may also have been induced: it is known to compete effectively with the heat release process.[29] We were able to avoid such a process, however, in our study by using a lower than threshold laser flux from the chosen cw laser output. The longer nanorod particles [AuNR(980); mean aspect ratio = 5.5] possess absorption cross sections that are nearly 3 times larger than those of AuNR(775) at their respective values of λ_{max}; at 785 nm, however, the temperature buildup from the longer nanorod particles (only 3.3 °C) is much lower than that of the shorter ones. This small temperature rise is due simply to the presence of a very low percentage of the shorter gold nanorods in the AuNR(980) suspension; these shorter nanorods provide a weak absorbance around the incident 785-nm light. To obtain an

absolute differentiation of the optothermal conversion effects of the two gold nanorod systems, it is necessary for the AuNR-(980) sample to exhibit total transparency to the incident wavelength. This situation can exist either by synthesis of particles that have a much narrower mean aspect ratio distribution or by longer gold nanorods that possess a value of λ_{max} further to the red. Again, it is clear that absorption of light by the particles is crucial for the temperature increase. We calculated the ideal rise in temperature for this system knowing that the light absorption by a 2 μL sample is 26 mW. The ideal temperature rise assumes a 100% photon-to-thermal energy conversion, and the heat release from this volume is a much slower process than the temperature buildup within the irradiation time (5 s). The relationship $E_{abs} = C_p mT$ gives $T =$ 15.5 °C. This value is quite close to the average temperature change within the sample aliquots, to a first-order approximation of $(26.2 + 3.5)/2 = 14.9$ °C. The implication of this agreement is that there is no other significant energy loss pathway competitive with the thermal release. A similar temperature rise (ca. 40 °C) for spherical gold nanoparticles (20-nm diameter) has been measured after their irradiation with a ca. 20 mW argon ion laser.[25] The wavelength-dependent photothermal effect can be further demonstrated by using a solid-state laser having an output at 981 nm. In this case, the AuNR(980) sample exhibited a higher temperature rise than did the shorter AuNR(775) sample. These experiments are sufficient to demonstrate that the optothermal conversion of the gold nanorods is highly efficient and that wavelength tuning is possible by making an appropriate selection of the particles' dimensions—or, more specifically, the particles' mean aspect ratios.

To further illustrate the importance of the absorbance of the sample at the specific wavelength of the chosen incident light, and its relationship to the resulting temperature rise, we conducted a series of measurements similar to those described above, but using in this case four AuNR(775) samples that had different spectral absorbances. The assembled results are presented in Figure 3. Experimentally, as employed in Figure 2, we placed the four AuNR(775) sample aliquots, depicted in Figure 3A, such that they were separated sufficiently to prevent any possible thermal image overlap. Their concentrations were adjusted carefully to give absorbances of 2.0, 1.5, 1.0, and 0.5 (Figure 3B). When examining the highest temperatures obtained in the thermal images of Figure 3C−F, we observe clearly that the thermal effect responds linearly to the concentration in Figure 3D−F, or more specifically to the particle concentration. In addition, thermal saturation is evident in the cases of the two samples having the highest concentrations (Figure 3C,D). A linear response is a reasonable finding, but unfortunately, further analysis of this experiment is limited in terms of the irradiation time and the concentration because of evaporation of the aqueous sample solutions.

In search of a much higher temperature increase and a more stable matrix, i.e., one that provides a better adiabatic system and stabilization effect on the gold nanorods, we implanted the gold nanorods into a transparent polyurethane material. The preconcentrated gold nanorods solutions were mixed with a water-soluble polyurethane (PU) and then each mixture was molded and dried to give uniform rectangular pieces. The concentrations of samples of both AuNR(750) and AuNR(1050) in PU were controlled such that they had similar absorbances at their respective absorption maxima, as indicated in Figure 4A,B. The poor thermal conductivity of PU and its ability to sustain higher temperatures make it a much better medium (relative to that of the aqueous milieu) to trap the thermal energy.

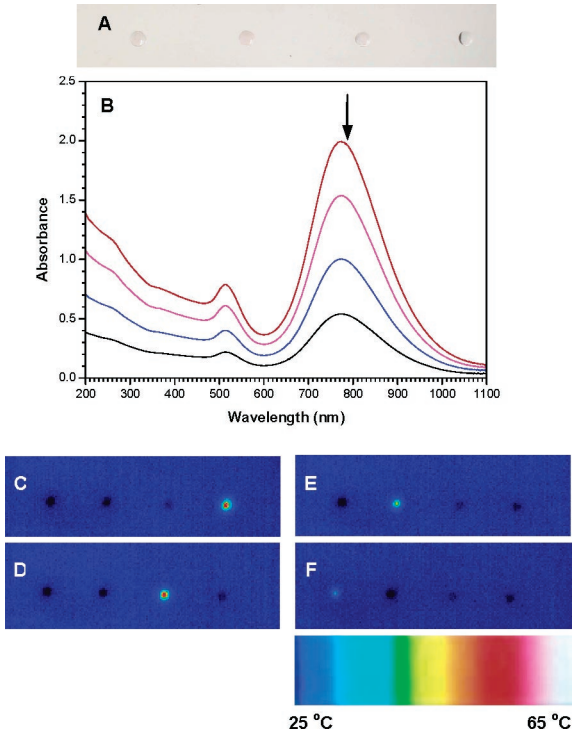

Figure 3. Dependence of optothermal conversion efficiency upon absorbance of the gold nanorods (mean aspect ratio = 3.9). (A) Photographic image of a slide upon which four sample droplets having absorbances (from right to left) of 2.0, 1.5, 1.0, and 0.5 were placed. (B) Absorption spectra of the four samples measured under an optical path length of 0.5 cm. The samples were illuminated using a continuous laser output similar in wavelength (represented by the downward arrow) and power to that described in Figure 1. The optothermal conversion image of each sample was recorded using an IR camera after irradiation for 5 s. (C)−(F) Thermal images of each of the four samples; the final temperatures at the centers of the hot spots are (C) 63.5 °C (absorbance = 2.0), (D) 57.7 °C (absorbance = 1.5), (E) 45.9 °C (absorbance = 1.0), and (F) 33.7 °C (absorbance = 0.5).

The blank sample of PU did not undergo any temperature change upon irradiation at 785 nm for 1 min (Figure 4C), but Figure 4D indicates that the temperature of AuNR(750) rose to as high as 106.9 °C under the same conditions. This remarkable optothermal conversion for an implanted gold nanorod system corresponds to a 79.4 °C increase in temperature. By examining the cooling of the AuNR(750) system after the laser had been turned off, we found that the temperature within the sample returns to the room temperature at very much the same rate as its heating occurred, i.e., within 1 min. This heating-and-cooling cycle repeats reproducibly, which demonstrates the extremely high stability[29] of the core gold nanorod particles supported by the solid matrix. Values of the highest temperatures it can reach during the measurements of repeating heating-and-cooling cycles are typically reproducible within less than 0.5 °C. Because of its much lower absorbance at 785 nm, the sample of AuNR-(1050) immobilized in the PU matrix exhibits a much less efficient optothermal conversion. The temperature change, as indicated in Figure 3E, was 39.9 °C. We believe that the optimal optothermal conversion efficiency of AuNR(1050) should occur selectively at an incident wavelength of ca. 1050 nm.

A similar optothermal effect has been demonstrated for gold nanoshells in in vivo MRTI analysis.[30] It revealed that nanoshell-treated tumors resulted in a more than 30 °C temperature increase on NIR exposure (820 nm; 35 W/cm^2) for 4−6 min. Our data simply indicate that, as optothermal convertors, gold nanorods exhibit a higher temperature change with shorter

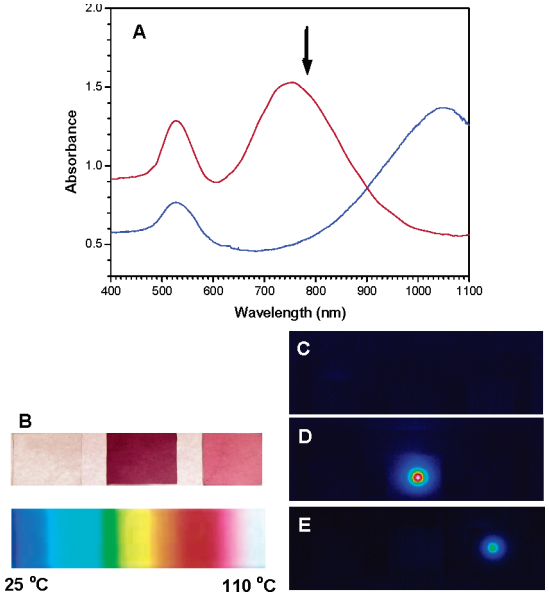

Figure 4. Optothermal conversion of gold nanorods in a PU matrix. (A) Absorption spectra of both AuNR(775) (mean aspect ratio = 3.8) and AuNR(1050) (mean aspect ratio = 5.5) nanorods in PU. (B) Photographic image displaying three PU pieces (1.5 × 1.5 × 0.2 cm). From left to right: neat PU, AuNR(750) in PU, and AuNR-(1050) in PU. The samples were illuminated using a continuous laser output similar in wavelength (represented by the downward arrow) and power to that described in Figure 1, and the IR camera recorded each image after 60 s irradiation. (C)−(E) Two-dimensional thermal images recorded for the three samples. The final temperatures at the centers of the illuminated areas are (C) 27.5, (D) 106.9, and (E) 67.4 °C.

irradiation time under similar laser conditions. It may be attributed directly to the difference of their intrinsic absorption coefficients. Furthermore, the measurements for the ultimate temperatures in the gold nanorods in PU system were limited in current studies due to the clear observation of the melting of PU. We believed that the gold nanorods, if embedded in suitable matrixes, can easily raise the temperatures beyond 110 °C under the cw laser irradiations without inducing the unwanted particle shape transformation.

4. Conclusions

The highly efficient optothermal conversion provided by gold nanorods is dependent on the wavelength. The highest temperatures can be reached effectively with these nanosystems by controlling either the particle concentration or the laser flux. An implication, based on their efficient optothermal conversion, may be that the gold nanorods can provide temporal temperature variations well above the highest ensemble temperature changes we have described in this paper. We have determined experimentally the melting temperature of the gold nanorods to be ca. 280 °C.[31] It will be interesting to discover whether these particles can attain superheating conditions; if they can, they will definitely have potential as contrast agents in optoacoustic biomedical imaging systems. Consequently, we believe that suitably conjugated gold nanorod based optothermal conversion systems will provide not only diagnostic but also therapeutic effects. It is known that the absorption cross sections and wavelength maxima of these nanoparticles are sensitive to the dielectric constant of the particle's nearest surrounding medium. It has been demonstrated[32] that these properties are affected by the adsorption of biomolecules onto a particle's surface; this finding suggests that these types of nanoparticles are potentially useful as biosensors. Our thermal imaging system, when employed as either aqueous droplets or as gold nanorods conjugated onto various biochip substrates, also has great potential for the future development of sensitive biodetection systems.

Acknowledgment. We thank Dr. A. Oraevsky for helpful discussions and Dr. S. H. Chang for help in arranging the equipment. Funding of this work by NSC Taiwan (Project Nos. NSC91-2120-M-001-001 and NSC92-2120-M-001-009) is gratefully acknowledged.

References and Notes

(1) Bruchez, M., Jr.; Moronne, M.; Gin, P.; Weiss, S.; Alivisatos, A. P. *Science* **1998**, *281*, 2013.
(2) Taylor, J. R.; Fang, M. M.; Nie, S. *Anal. Chem.* **2000**, *72*, 1979.
(3) Han, M.-Y.; Gao, X.; Su, J. Z.; Nie, S. *Nat. Biotech.* **2001**, *19*, 631.
(4) Chan, W. C. W.; Nie, S. *Science* **1998**, *281*, 2016.
(5) Bohren, C. F.; Huffman, D. R. *Absorption and Scattering of Light by Small Particles*; Wiley: New York, 1983.
(6) Elghanian, R.; Storhoff, J. J.; Mucic, R. C.; Letsinger, R. L.; Mirkin, C. A. *Science* **1997**, *277*, 1078.
(7) Storhoff, J. J.; Elghanian, R.; Mucic, R. C.; Mirkin, C. A.; Letsinger, R. L. *J. Am. Chem. Soc.* **1998**, *120*, 1959.
(8) Storhoff, J. J.; et al. *J. Am. Chem. Soc.* **2000**, *122*, 4640.
(9) Reynolds, R. A., III; Mirkin, C. A.; Letsinger, R. L. *J. Am. Chem. Soc.* **2000**, *122*, 3795.
(10) Cao, Y. W.; Jin, R.; Mirkin, C. A. *J. Am. Chem. Soc.* **2001**, *123*, 7961.
(11) Taton, T. A.; Mirkin, C. A.; Letsinger, R. L. *Science* **2000**, *289*, 1757.
(12) Taton, T. A.; Lu, G.; Mirkin, C. A. *J. Am. Chem. Soc.* **2001**, *123*, 5164.
(13) Nam, J.-M.; Park, S.-J.; Mirkin, C. A. *J. Am. Chem. Soc.* **2002**, *124*, 3820.
(14) Nam, J.-M.; Thaxton, C. S.; Mirkin, C. A. *Science* **2003**, *301*, 1884.
(15) Park, S.-J.; Taton, T. A.; Mirkin, C. A. *Science* **2002**, *295*, 1503.
(16) Boyd, G. T.; Yu, Z. H.; Shen, Y. R. *Phys. Rev. B* **1986**, *33*, 7923.
(17) Van Duyne, R. P. In *Chemical and Biochemical Applications of Lasers*; Moore, C. B., Ed.; Academic Press: New York, 1979; Vol. 4, pp 101−185.
(18) Moskovits, M. *Rev. Mod. Phys.* **1985**, *47*, 783.
(19) Doering, W. E.; Nie, S. *J. Phys. Chem. B* **2002**, *106*, 311.
(20) Nie, S.; Emory, S. R. *Science* **1997**, *275*, 1102.
(21) Antoine, R.; Brevet, P. F.; Girault, H. H.; Bethell, D.; Schiffrin, D. J. *Chem. Commun.* **1997**, *19*, 1901.
(22) Ahmadi, T. S.; Logunov, S. L.; El-Sayed, M. A. *J. Phys. Chem.* **1996**, *100*, 8053.
(23) Logunov, S. L.; Ahmadi, T. S.; El-Sayed, M. A.; Khoury, J. T.; Whetten, R. L. *J. Phys. Chem. B* **1997**, *101*, 3713.
(24) Kamat, P. V.; Shanghavi, B. *J. Phys. Chem. B* **1997**, *101*, 7675−7679.
(25) Boyer, D.; Tamarat, P.; Maali, A.; Lounis, B.; Orrit, M. *Science* **2002**, *297*, 1160.
(26) Hamad-Schifferli, K.; Schwartz, J. J.; Santos, A. T.; Zhang, S.; Jacobson, J. M. *Nature* **2002**, *415*, 152.
(27) This value was determined by knowing exactly (a) the number of nanoparticles in a given volume of suspended solution, obtained by TEM imaging on a copper grid, and (b) their absorbance. The former determines the particle concentration of the gold nanorods, and the latter can then be used to calculate the absorption coefficient. Thus, we calculated the absorption coefficient of Au nanorods at 950 nm to be 5×10^9 L·(mol of particles)$^{-1}$·cm^{-1} for particles having their surface plasmon band at $\lambda_{max} = 950$ nm.
(28) Yu, Y. Y.; Chang, S. S.; Lee, C. L.; Wang, C. R. C. *J. Phys. Chem. B* **1997**, *101*, 6661.
(29) Chang, S. S.; Shih, C. W.; Chen, C. D.; Lai, W. C.; Wang, C. R. C. *Langmuir* **1999**, *15*, 701.
(30) Hirsch, L. R.; Stafford, R. J.; Bankson, J. A.; Sershen, S. R.; Rivera, B.; Price, R. E.; Hazle, J. D.; Halas, N. J.; West, J. L. *Proc. Natl. Acad. Sci. U.S.A.* **2003**, *100*, 13549.
(31) We measured the melting temperature of the gold nanorods by using TEM coupled with a thermal probe. Particles on the sample grid were heated at several temperatures prior to taking their images. We believe that the value measured is a lower limit of their true melting temperature because of the limitations of this method of measurement and the samples' environment.
(32) Nath, N.; Chilkoti, A. *Anal. Chem.* **2002**, *74*, 504.